International Journal of Thermophysics, Vol. 20, No. 4, 1999

Fast Melting of Amorphous Silicon Carbide Induced by Nanosecond Laser Pulse[1]

P. Baeri,[2,3] C. Spinella,[4] and R. Reitano[2]

We report the first experimental detailed study of laser induced surface melting on the nanoscale time scale of amorphous silicon carbide layers produced by ion implantation. Time-resolved reflectivity has been used to observe the fast liquid–solid–liquid transition features, and transmission electron microscopy (TEM) was used in order to study the structure resulting after the fast solidification following the laser induced melting. By means of the evaluation of the laser fluences required to induce melting of amorphous layers of different thickness on top of a crystalline substrate, we evaluated the thermal diffusion coefficient and the melting point of the amorphous material which occurred much lower than for crystalline material. Moreover, we give evidence of amorphous-to-crystal transitions occurring in the solid phase on the nanosecond time scale, for laser irradiation at fluences below the melting threshold. A quite different crystalline structure is observed for crystallization from the liquid phase than from the solid phase.

KEY WORDS: laser melting; silicon carbide.

1. INTRODUCTION

Pulsed laser treatment of a solid surface has two major features: fast heating up to the melting point on the nanosecond time scale and subsequent rapid solidification and cooling. Although it was first successfully used to anneal the surface damage produced by ion implantation in single crystal silicon [1], it was soon recognized that fast surface melting is a powerful probe of the high-temperature properties of metastable phases.

[1] Paper presented at the Fifth International Workshop on Subsecond Thermophysics, June 16–19, 1998, Aix en Provence, France.

[2] Dipartimento di Fisica, Università di Catania and Istituto Nazionale di Fisica della Materia, UdR Catania, Corso Italia 57, I-95129 Catania, Italy.

[3] To whom correspondence should be addressed.

[4] CNR-IMETEM, Stradale Primosole 50, I-95100 Catania, Italy.

0195-928X/99/0700-1211$16.00/0 © 1999 Plenum Publishing Corporation

In the nanosecond time domain, the diffusion length of most atomic species in the solid phase is a fraction of the interatomic distance. Hence, a metastable phase can be heated up to its equilibrium point with the liquid phase and melted, bypassing any solid phase transformation or decomposition. In this work we show melting of amorphous silicon carbide layer bypassing both its crystallization and its peritectic decomposition.

The pulsed laser irradiation technique has also an advantage due to the planar geometry of the process. Owing to the large optical absorption coefficient and the small heat diffusion length during the irradiation time, the thickness of the material involved in the heating process is of the order of a few hundred nanometers, whereas the lateral extension of the laser beam spot is generally several millimeters. The resulting structure is then suitable to be analyzed with all of the powerful techniques that have been developed for thin-film analysis. Moreover, some time-resolved analytical methods have been developed in order to follow the transition in real time.

Optical probing is the more widely used method. The melt duration can be determined from reflectance measurements for materials with very different liquid- and solid-state reflectivities [2] such as, for example, a semiconductor. Optical probing has also been shown to be a precise and sensitive method of detecting the initiation of surface melting [3]. Hence, the value of the laser fluence for which the melting temperature is reached on the irradiated sample surface can be experimentally measured. A knowledge of this value, called the melting threshold, allows the evaluation of the melting temperature and other thermal properties related to heat diffusion as has been shown in the case of supersaturated Si–As solid solutions [4] and of amorphous silicon [5].

Silicon carbide (SiC) is a semiconductor for which technological interest is increasingly growing. Its amorphous phase exhibits luminescence properties in the visible region of wavelengths that are very promising for developing optoelectronic devices, and much work has been devoted to the fabrication and characterization of SiC amorphous thin films [6]. Silicon carbide exhibits a peritectic decomposition at 2840 K and the crystal–liquid equilibrium temperature has been estimated to be 3500 K [7].

In this work we use the pulsed laser heating technique and transient reflectivity measurements to evaluate the melting point and the thermal diffusion coefficient for amorphous silicon carbide (a-SiC) produced by ion implantation.

2. EXPERIMENTAL

6H SiC single crystal wafers with the surface normally oriented with respect to the *c*-axis of the hexagonal lattice were implanted with Ar^+ ions

with energies ranging from 50 to 300 KeV and doses between 5×10^{14} and 5×10^{15} ions $\cdot$ cm^{-2} in order to produce amorphous layers of different thickness on top of the wafers. The thickness of the amorphous layer produced by the 300-keV ion implantation was measured by both 2-MeV He^{+} Rutherford backscattering spectrometry (RBS) under channeling condition along the *c*-axis of the substrate and by transmission electron microscopy (TEM) with a 400-kV JEOL microscope. It resulted in 300 nm in the latter case and 3×10^{18} atoms $\cdot$ cm^{-2} in the former, for which we estimate a value of 10^{23} atoms $\cdot$ cm^{-2} for the density of the amorphous layer, i.e., the same as of the crystal, which corresponds to 3.2 g $\cdot$ cm^{-2}. Samples implanted with other energies of the Ar^{+} beam resulted in amorphous layers thicknesses of 60, 80, 100, 120, and 200 nm. Samples were successively irradiated with a Q-switched ruby laser ($\lambda = 694$ nm) with 25-ns pulse duration and fluence ranging from 0.1 to 1 J $\cdot$ cm^{-2}.

Spatial homogeneity on a 3-mm-diameter circular spot of the laser beam was achieved by using a bent quartz rod light homogenizer. Microinhomogeneities are not completely avoided with this method so that lateral fluctuations of the laser light intensity of the order of 10% are still present on the micron scale.

A 15-mW cw argon laser (488-nm wavelength), focused on the sample surface in the middle of the ruby laser spot, was used in order to probe the sample reflectivity. Since the reflectivity in the visible region of the liquid SiC is expected to be much higher than the one of solid SiC, this method is used in order to monitor the occurrence of the liquid phase on the sample surface. The argon laser beam was polarized parallel to the plane of incidence and was incident on the sample surface at an angle of about 70°, which is very close to the Brewster angle for solid SiC. This choice enhances the ratio between the solid and the liquid reflectivities.

The reflected Ar laser beam intensity was measured during the ruby laser irradiation and then by a fast p-i-n photodiode and registered in a digital oscilloscope with a few nanoseconds time resolution. After irradiation, the same samples were observed by TEM in cross-sectional configuration.

3. TRANSIENT REFLECTIVITY RESULTS

In Fig. 1 the reflectivity signals for the 300-nm-thick amorphous layer sample are reported for several ruby laser fluences. On the time scale in the figure, the peak of the ruby laser pulse corresponds to the time $t = 15$ ns. For fluences less than 0.3 J $\cdot$ cm^{-2}, the reflectivity signal does not change during the irradiation indicating that no melting occurred. For 0.67 J $\cdot$ cm^{-2} fluence irradiation, however, the reflectivity exhibits a plateau

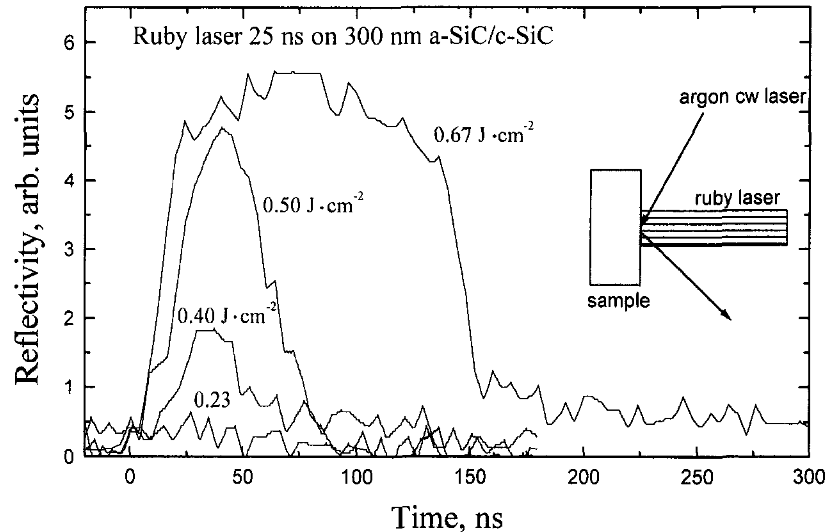

Fig. 1. Transient reflectivity signals obtained from a cw argon laser during the irradiation with a 25-ns ruby laser pulse on the surface of a 300-nm-thick amorphous SiC layer on top of a crystalline SiC substrate for several values of the ruby laser fluence. The peak of the ruby laser pulse is at approximately 15 ns.

indicating that the sample surface stayed molten for a time interval of about 150 ns.

For intermediate fluence values, the reflectivity during the irradiation does not reach the value of the molten SiC. This is due both to the micron-size inhomogeneities of the ruby laser beam, which, in turn, results in a nonuniform melt surface and to the fact that the molten layer may have a smaller thickness than the light absorption depth of the probe wavelength in the liquid SiC (about 10 nm). The so-called melting threshold is the minimum value of the laser fluence (E_{th}) for which the melting point is reached at the sample surface, when the melting process starts.

E_{th} is experimentally evaluated using a value of the laser fluence a little smaller than the one for which the average value of solid and liquid SiC (i.e., the one obtained when the plateau, as reported in Fig. 1, for the $0.67\ \mathrm{J \cdot cm^{-2}}$ irradiation is observed) is reached by the transient reflectivity signal [3]. For the case reported in Fig. 1, $E_{th} = 0.4\ \mathrm{J \cdot cm^{-2}}$.

The maximum value reached by the time-resolved reflectivity as a function of the laser fluence is reported in Fig. 2 for two samples: 60- and 300-nm-thick amorphous layers. To induce melting in the thinner amorphous layer sample, much higher laser fluences are needed. From the data

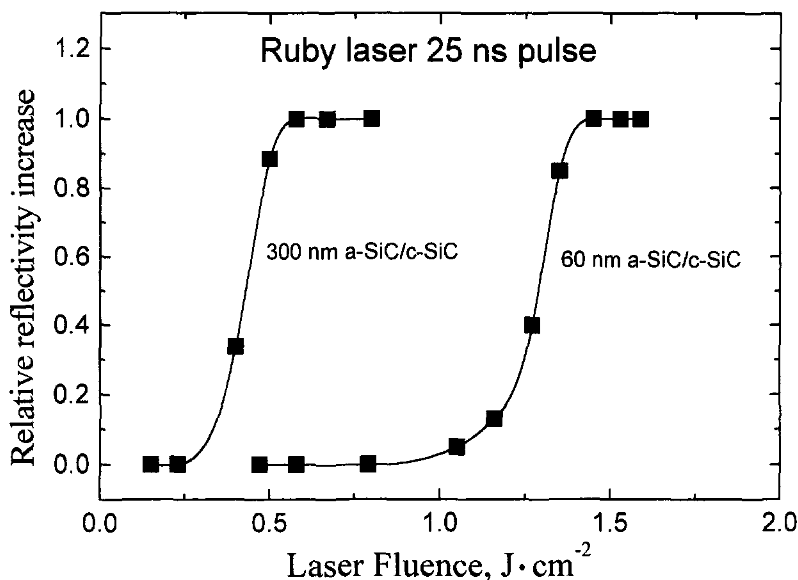

Fig. 2. Maximum value of the reflectivity during the transient, normalized to that of the liquid SiC, versus the ruby laser fluence for samples with a 300- and 60-nm-thick amorphous SiC layer, respectively.

in Fig. 2, the evaluated melting thresholds are 1.3 and 0.4 $J \cdot cm^{-2}$ for the 60- and 300-nm-thick amorphous layers, respectively.

The melting thresholds as a function of the amorphous layer thickness for all samples are reported in Fig. 4 as filled circles. Error bars have been evaluated from the statistical analysis of the set of curves such as those in Fig. 2 and from the uncertainties in the laser fluence calibration. The dashed curve in Fig. 4 is the result of computations discussed below.

3.1. Evaluation of Thermal Parameters of Amorphous SiC

The basic processes involved during pulsed laser melting are heat generation by the light absorbed in the proximity of the sample surface and cooling by heat transport toward the cold substrate.

The absorbed energy is instantaneously (i.e., on the picosecond time scale) converted into heat which diffuses according to heat conduction laws.

The heat diffusion equation, with an additional source term that represents the laser heating and with appropriate boundary conditions to account for phase transformations, sample geometry, and structure, has been extensively used to predict and model heating, melting, and

resolidification of metal and semiconductor surface layers following pulsed laser irradiation [8].

In our geometry the diffusion equation is unidimensional:

$$\frac{\partial T}{\partial t} = \frac{\alpha}{\rho c} I(z, t) + \frac{\partial}{\partial z}\left(D \frac{\partial T}{\partial z}\right)$$

where T is the temperature as function of time t and depth z into the sample, α is the light absorption coefficient, ρ is the mass density, c is the specific heat, $I(z, t)$ is the laser light intensity as a function of time inside the sample, and D is the thermal diffusivity. Without going into details of the solution of the heat diffusion equation, only those aspects related to the relationship between the melting threshold and the thermal properties and structure of our samples are discussed here.

The light absorption coefficient at the ruby laser wavelength for our ion-implanted amorphous SiC is $4.5 \times 10^4\ \mathrm{cm}^{-1}$ [9], while crystalline SiC is practically transparent. Moreover, the thermal diffusivity along the c-axis direction of crystal SiC is very large, ranging from $1.2 \cdot \mathrm{cm}^2 \cdot \mathrm{s}^{-1}$ at room temperature to $0.1\ \mathrm{cm}^2 \cdot \mathrm{s}^{-1}$ at 2800 K [10], while for the amorphous material a much smaller value is expected, as it has been measured, for example, for amorphous silicon [5].

For these reasons, during the heating by the laser pulse a very steep temperature gradient is formed close to the amorphous–crystal interface, and it is increasingly steeper with a decrease in the amorphous layer thickness.

The crystal substrate is heated only by heat conduction, which, in turn, is governed by the temperature gradient at the amorphous–crystal interface. With an increase in the value of this gradient, the heat flow from the heated amorphous layer will increase, the crystal will became warmer, and consequently, the amorphous layer will cool. For this reason, we observe the melting threshold to increase with a decrease in the amorphous layer thickness.

On the other hand, if the amorphous layer thickness is much larger then the heat diffusion length ($=\sqrt{D\tau}$) during the heating pulse duration τ, all of the energy remains stored in the amorphous layer. The temperature profile will not change with the amorphous thickness, and neither will the melting threshold.

For our experimental data, this is observed when the amorphous layer is thicker than 200 nm (see Fig. 4) so that an upper limit of $10^{-2}\ \mathrm{cm}^2 \cdot \mathrm{s}^{-1}$ for D is estimated. A precise evaluation of the influence of the amorphous layer thickness on the temperature rise has been done by solving the heat diffusion equation. The following values for the parameters were adopted:

$\alpha = 4.5 \times 10^4\ \mathrm{cm}^{-1}$ and 0 for amorphous and crystal, respectively,
$c = 1.3\ \mathrm{J \cdot g^{-1} \cdot K^{-1}}$ for both amorphous and crystal,
$\rho = 3.2\ \mathrm{g \cdot cm^{-3}}$ for both amorphous and crystal, and
D depending on T as from Ref. 10 for crystal.

As an example, in Fig. 3 the calculated maximum temperature reached on the surface of a sample with 60-nm (dashed lines)- and 300-nm (solid lines)-thick amorphous layers versus the ruby laser fluence is reported for two D values for amorphous SiC. In all cases the temperature increases linearly with the fluence, and moreover, as discussed before, the temperature for the same laser fluence is considerably higher for the sample with the thicker amorphous layer.

The rate of temperature increase also depends strongly on the selected value of D. In fact, for $D = 2.5 \times 10^{-3}\ \mathrm{cm^2 \cdot s^{-1}}$, it is almost a factor of four greater than for $D = 2.5 \times 10^{-2}\ \mathrm{cm^2 \cdot s^{-1}}$ in the case of the 60-nm-thick amorphous layer. This factor becomes two in the case of a 300-nm-thick amorphous layer. These calculations, together with the experimental values of the melting threshold for the full range of amorphous layer thickness, allow the evaluation of both D and the melting temperature of the amorphous silicon carbide.

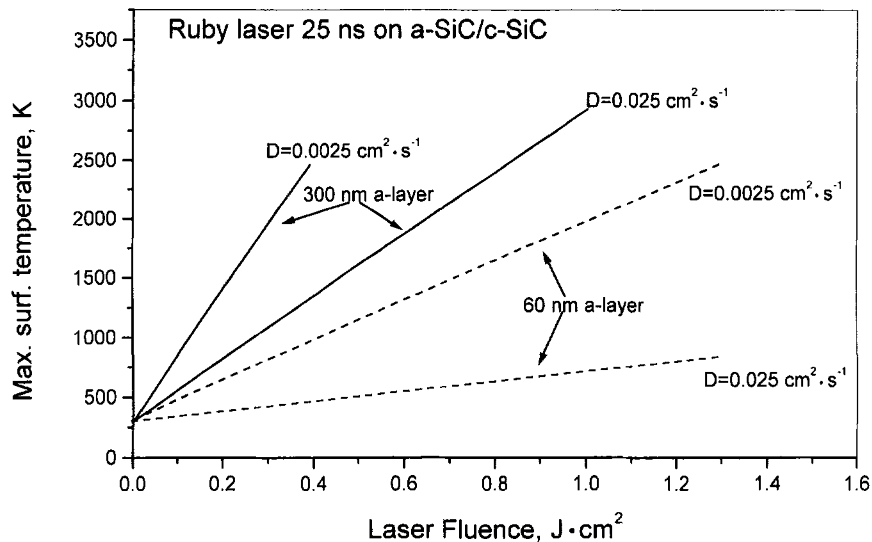

Fig. 3. Calculated maximum temperature on the sample surface during irradiation with a 25-ns ruby laser pulse as a function of the laser fluence for samples with 300-nm (solid lines)- and 60-nm (dashed lines)-thick amorphous SiC layers and for two values of the amorphous SiC thermal diffusion coefficient D.

The melting temperature T_m is evaluated from the curves in Fig. 3 as the maximum temperature reached on the surface for the experimental value of the fluence for which the surface melting is observed, i.e., the melting threshold. T_m must be the same for all the amorphous layer thicknesses, provided that the correct value of D is used.

For example, in the data reported in Fig. 3, with $0.4\ \mathrm{J \cdot cm^{-2}}$ the melting threshold for the 300-nm-thick amorphous layer sample, T_m is about 2450 K assuming $D = 2.5 \times 10^{-3}\ \mathrm{cm^2 \cdot s^{-1}}$ but about 1250 K for the higher value of D. For the 60-nm-thick amorphous layer sample at the experimental threshold of $1.3\ \mathrm{J \cdot cm^{-2}}$, the estimated T_m is only 750 K if $D = 2.5 \times 10^{-2}\ \mathrm{cm^2 \cdot s^{-1}}$ is adopted, while it is every close to 2450 K when $D = 2.5 \times 10^{-3}\ \mathrm{cm^2 \cdot s^{-1}}$ is assumed. The latter values of D and T_m therefore, are very close to agree with our experimental results. By means of a complete least-squares fit procedure, involving the diffusion equation and the experimental data in Fig. 4, the following values of D and T_m are found:

$$T_m = 2445 \pm 320\ \mathrm{K} \quad \text{and} \quad D = (2.46 \pm 0.15) \times 10^{-3}\ \mathrm{cm^2 \cdot s^{-1}}$$

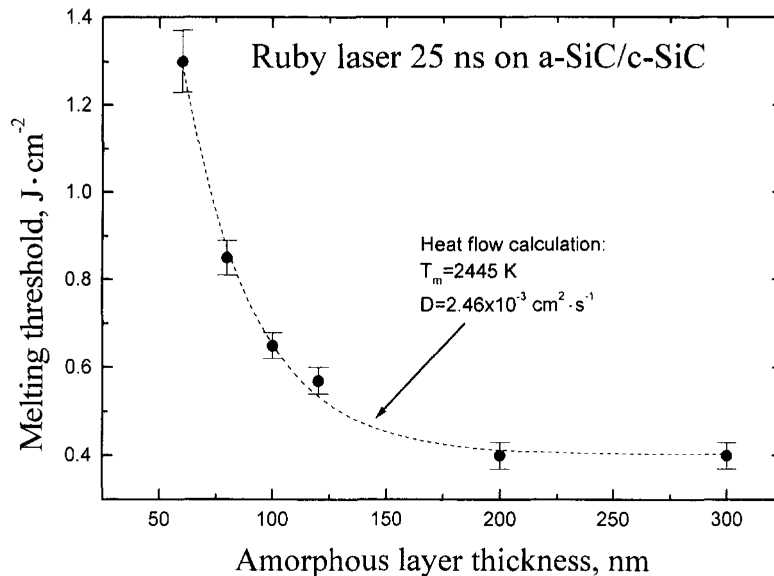

Fig. 4. (●) Measured melting threshold for a 25-ns pulsed ruby laser irradiation of samples of crystalline SiC with an amorphous SiC layer on top as a function of the amorphous layer thickness. Dashed line: result of heat flow calculation assuming the melting temperature T_m and the diffusion coefficient D given in the figure.

The relative error in the melting point is larger than that for the thermal diffusivity since it reflects the experimental uncertainties in the ruby laser light absorption coefficient in the amorphous SiC and in its specific heat, while these parameters do not affect the value of D, which, instead, is determined primarily by the slope of variation of the melting threshold with the amorphous layer thickness. The dashed curve in Fig. 4 represents the result of our heat flow calculation with the best-fit values of D and T_m indicated above.

4. TRANSMISSION ELECTRON MICROSCOPY RESULTS

The cross-sectional TEM of the 300-keV Ar^+ implanted, $1\ J \cdot cm^{-2}$ irradiated sample is shown in lower part in Fig. 5. For comparison, in the upper part of Fig. 5 the as-implanted sample is also shown. The irradiated sample results in a bilayered structure with an amorphous layer 100 nm

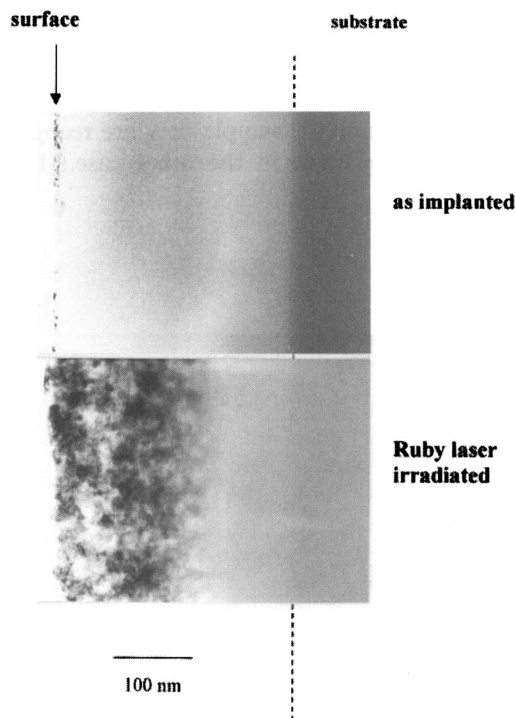

Fig. 5. Cross-sectional TEM image of a 300-nm-thick amorphous SiC layer on top of SiC single crystal obtained by Ar^+ ion implantation. As implanted (upper) and after irradiation with a $1\text{-J} \cdot cm^{-2}$, 25-ns ruby laser pulse (lower).

thick buried below a polycrystalline layer 200 nm thick. The latter observation results from the solidification of the liquid layer created during the laser irradiation and presents an average grain size of about 30 nm almost independent of depth, with a sharp interface with the underlying amorphous layer.

Electron diffraction patterns from this polycrystalline layer are shown in Fig. 6a. Figure 6b, instead, refers to a sample which has been irradiated with 50 shots of $0.3\ J \cdot cm^{-2}$ ruby laser pulse. For the latter case, the laser fluence is below the melting threshold, and indeed, evidence of melting has not been observed by transient reflectivity measurements during the irradiation. Although after one-shot irradiation the sample is still amorphous, after many shots we observed through cross-sectional TEM a polycrystalline structure at the surface with an average grain size of 20 nm, which becomes progressively thinner on going inside the sample, until, at about 100 nm depth, it remains indistinguishable from the amorphous layer.

The diffraction pattern of the topmost polycrystalline layer is shown in Fig. 6b. The diffraction rings of the two samples looks quite different. Indeed for the $1\ J \cdot cm^{-2}$ irradiated sample they are recognized to be those of the cubic 3C SiC lattice, while in the other case, they belong to the hexagonal SiC lattice.

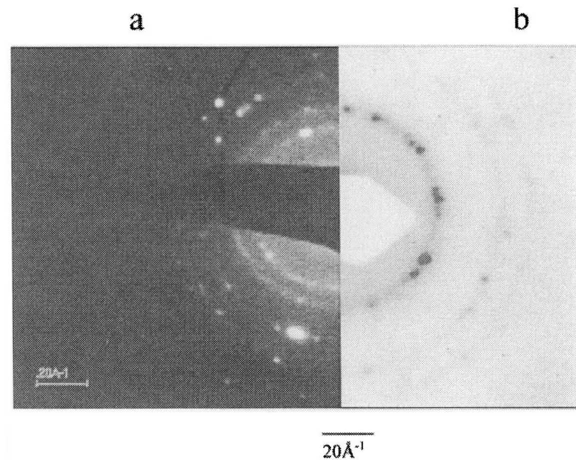

Fig. 6. The 400-keV electron diffraction pattern from (a) the polycrystalline layer of the sample in Fig. 2 (lower) and (b) a similar sample but irradiated with 50 consecutive $0.3\text{-}J \cdot cm^{-2}$, 25-ns ruby laser pulses.

5. SUMMARY AND CONCLUSION

In conclusion, we have shown that during a single-shot 25-ns ruby laser irradiation, amorphous SiC does not exhibits solid phase transformation to the crystal phase so that it can reach its equilibrium temperature with the liquid SiC and melt. Subsequent resolidification results in a polycrystalline structure.

The observation by transient reflectivity measurements of the melt onset, together with heat flow calculations based on the heat diffusion equation, allowed the determination of the melting point and of the thermal diffusivity, properties that are not measurable in the steady-state condition for a metastable phase such as amorphous SiC. With a longer heating time, in fact, the amorphous phase will transform to a crystal before melting. Indeed, we observed an amorphous–crystal solid-phase transition after laser irradiation but with more than one order of magnitude in the time duration of the laser exposure (50 shots). The crystal phase obtained from the amorphous phase from solid phase transformation is different from the one obtained by the solidification of the liquid phase. The obtained value of the a-SiC melting point (2445 K) is much lower than that for the crystal phase (3500 K) and even lower than the peritectic decomposition point (2850 K).

REFERENCES

1. G. Foti, E. Rimini, G. Vitali, and M. Bertolotti, *Appl. Phys.* **14**:186 (1977).
2. D. Auston, J. Golovchenko, A. Simon, and C. Surke, *Appl. Phys. Lett.* **34**:777 (1979).
3. P. Baeri, M. Grimaldi, and R. Reitano, *High Temp.-High Press.* **23**:675 (1991).
4. P. Baeri, R. Reitano, M. Malvezzi, and A. Borghesi, *J. Appl. Phys.* **67**:1801 (1990).
5. M. Grimaldi, P. Baeri, M. Malvezzi, and C. Sirtori, *Int. J. Thermophys.* **13**:141 (1992).
6. F. Demichelis, F. Giorgis, F. Pirri, and E. Tresso, *Physica B* **225**:103 (1996).
7. R. Reitano and P. Baeri, *Int. J. Thermophys.* **17**:1079 (1996).
8. P. Baeri and E. Rimini, *Mat. Chem. Phys.* **46**:169 (1996).
9. P. Musumeci, R. Reitano, L. Calcagno, F. Roccaforte, A. Makhtari, and M. Grimaldi, *Phil. Mag. B* **76**:323 (1997).
10. G. Slack, *J. Appl. Phys.* **35**:3460 (1964).